by AFOSR Grant 84-0428, and on the San Diego Supercomputer Center Cray X-MP (time provided by the NSF). The authors are most grateful to P. J. MacDougall and R. F. W. Bader for providing their AIMPAC program for computing bent bond lengths and to Professor H. F. Schaefer III and Dr. Roger Grev for providing us with a preprint of their paper prior to its publication.

Appendix

Consider an arc length a joined by a segment of length L as shown in Figure 2. The boundary conditions are

$$\left(\frac{dy}{dx}\right)_{x=0} = S_1, \quad \left(\frac{dy}{dx}\right)_{x=L} = -S_2 \tag{A1}$$

In general, we assume the slope of the arc varies linearly, so

$$\frac{dy}{dx} = S_1 - kx \tag{A2}$$

$$\left(\frac{dy}{dx}\right)_{x=L} = S_1 - kL = -S_2 \tag{A3}$$

So,

$$k = \frac{S_1 + S_2}{L}; \quad \frac{dy}{dx} = S_1 - \frac{(S_1 + S_2)}{L}x \tag{A4}$$

Now, by definition of arc length,

$$d\lambda = \left[1 + \left(\frac{dy}{dx}\right)^2\right]^{1/2} dx$$

$$d\lambda = \left[1 + S_1^2 - \frac{2S_1(S_1 + S_2)}{L}x + \frac{(S_1 + S_2)^2x^2}{L^2}\right]^{1/2} dx$$

Integrating $d\lambda$ from 0 to L and rearranging gives eq 4 in the text.

Supplementary Material Available: Tables of harmonic frequencies for cyclopropane, cyclobutane, cyclopentane, cyclohexane, silacyclopropane, silacyclobutane, silacyclopentane, and silacyclohexane (8 pages). Ordering information is given on any current masthead page.

Band Electronic Structure of the Lithium Molybdenum Purple Bronze $Li_{0.9}Mo_6O_{17}$

Myung-Hwan Whangbo*[1a] and Enric Canadell*[1b]

Contribution from the Department of Chemistry, North Carolina State University, Raleigh, North Carolina 27695-8204, and the Laboratoire de Chimie Théorique, Université de Paris-Sud, 91405 Orsay, France. *Received May 21, 1987*

Abstract: The electronic structure of $Li_{0.9}Mo_6O_{17}$ was examined by performing tight-binding band calculations, and the calculated band electronic structure was analyzed in terms of orbital interaction analysis. $Li_{0.9}Mo_6O_{17}$ is three-dimensional in crystal structure but pseudo-one-dimensional (1D) in electrical properties, because the partially filled d-block bands of $Li_{0.9}Mo_6O_{17}$ originate primarily from the Mo_4O_{18} chains embedded in the Mo_4O_{15} octahedral layers. Of the four filled d-block bands of $Li_{0.9}Mo_6O_{17}$, two partially filled bands are dispersive along the Mo_4O_{18} direction. Each of these two bands provides an identical 1D Fermi surface nested by the vector $\mathbf{q} \cong (0,0.45b^*,0)$. Therefore, it is likely that $Li_{0.9}Mo_6O_{17}$ is susceptible to either a charge or spin density wave formation associated with the nesting vector. The resistivity upturn at 25 K and the superconductivity at ~1.9 K in $Li_{0.9}Mo_6O_{17}$ were discussed on the basis of the calculated Fermi surfaces.

Molybdenum purple bronzes $A_{0.9}Mo_6O_{17}$ ($A = K$[2], Na[3]) and $TlMo_6O_{17}$[4] are two-dimensional (2D) metals and exhibit a charge density wave (CDW) phenomenon. $K_{0.9}Mo_6O_{17}$ consists of metal-oxygen layers of composition Mo_6O_{17}, constructed from MoO_6 octahedra and MoO_4 tetrahedra by sharing their oxygen corners, and the K^+ cations lie in between such Mo_6O_{17} layers.[2a] This 2D character of the crystal structure gives rise to the 2D metallic properties of $K_{0.9}Mo_6O_{17}$. In structure and physical properties, $Na_{0.9}Mo_6O_{17}$[3] and $TlMo_6O_{17}$[4] are similar to $K_{0.9}Mo_6O_{17}$.[2] However, it is not the case with $Li_{0.9}Mo_6O_{17}$.[5] This lithium purple bronze has a three-dimensional (3D) crystal structure, but it exhibits pseudo-one-dimensional (1D) metallic character,[5] eventually becoming a superconductor at ~2 K.[5] Furthermore $(Li_{1-x}Na_x)_{0.9}Mo_6O_{17}$ (≤0.48) and $(Li_{1-x}K_x)_{0.9}Mo_6O_{17}$ ($x \leq 0.40$) exhibit superconductivity at ~2 K[5d,e] despite random potentials expected from the presence of mixed alkali cations. To gain some insight into these apparently puzzling structural and electrical properties of $Li_{0.9}Mo_6O_{17}$, we examine the electronic structure of $Li_{0.9}Mo_6O_{17}$ by performing tight-binding band calculations[6,7] based upon the extended-Hückel method.[8] The atomic

(1) (a) Department of Chemistry, North Carolina State University, Raleigh, NC 27695-8204. (b) Laboratoire de Chimie Théorique, Bât. 490, Université de Paris-Sud, 91405 Orsay Cedex, France.

(2) (a) Vincent, H.; Ghedira, M.; Marcus, J.; Mercier, J.; Schlenker, C. *J. Solid State Chem.* **1983**, *43*, 113. (b) Buder, R.; Devenyi, J.; Dumas, J.; Marcus, J.; Mercier, J.; Schlenker, C. *J. Phys. (Les Ulis, Fr.)* **1982**, *43*, L59. (c) Bervas, E.; Cochrane, R. W.; Dumas, J.; Escribe-Filippini, C.; Marcus, J.; Schlenker, C. *Lect. Notes Phys.* **1985**, *217*, 144. (d) Dumas, J.; Bervas, E.; Marcus, J.; Salomon, D.; Schlenker, C. *J. Mag. Magn. Mater.* **1983**, *31-34*, 535. (e) Escribe-Filippini, C.; Konate, K.; Marcus, J.; Schlenker, C.; Almairac, R.; Ayroles, R.; Roucau, R. *Philos. Mag. B* **1984**, *50*, 321.

(3) (a) Gatehouse, B. M.; Lloyd, D. J.; Miskin, B. K. *NBS Spec. Publ. (U.S.)* **1972**, *No. 364*, 15. (b) Stephenson, N. C. *Acta Crystallogr.* **1966**, *20*, 59. (c) Greenblatt, M.; Ramanujachary, K. V.; McCarroll, W. H.; Neifeld, R.; Waszczak, J. V. *J. Solid State Chem.* **1985**, *59*, 149.

(4) (a) Ganne, M.; Dion, M.; Boumaza, A.; Tournoux, M. *Solid State Commun.* **1986**, *59*, 137. (b) Ramanujachary, K. V.; Collins, B. T.; Greenblatt, M. *Solid State Commun.* **1986**, *59*, 647.

(5) (a) Onoda, M.; Toriumi, K.; Matsuda, Y.; Sato, M. *J. Solid State Chem.* **1987**, *66*, 163. (b) Schlenker, C.; Schwenk, H.; Escribe-Filippini, C.; Marcus, J. *Physica* **1985**, *135B*, 511. (c) Greenblatt, M.; McCarroll, W. H.; Neifeld, R.; Croft, M.; Waszczak, J. V. *Solid State Commun.* **1984**, *51*, 671. (d) Ramanujachary, K. V.; Collins, B. T.; Greenblatt, M.; McNally, P.; McCarroll, W. H. *Solid State Ionics* **1986**, *22*, 105. (e) Matsuda, Y.; Onoda, M.; Sato, M. *Physica* **1986**, *143B*, 243. (f) Sato, M.; Matsuda, Y.; Fukuyama, H. *J. Phys. C*, submitted for publication.

(6) Whangbo, M.-H.; Hoffmann, R. *J. Am. Chem. Soc.* **1978**, *100*, 6093.

(7) Whangbo, M.-H.; Schneemeyer, L. F. *Inorg. Chem.* **1986**, *25*, 2424 and references cited therein for details of our tight binding calculations.

0002-7863/88/1510-0358$01.50/0

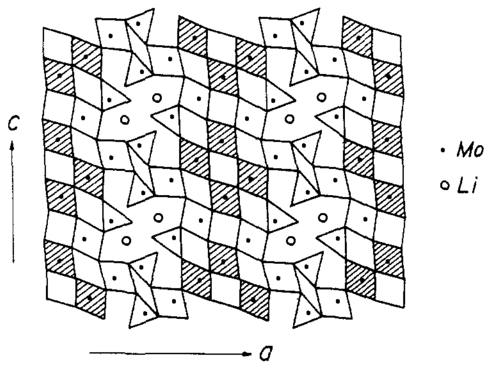

Figure 1. A schematic drawing of the crystal structure of $Li_{0.9}Mo_6O_{17}$, where each triangle or tetragon with an Mo atom represents an MoO_4 tetrahedron or octahedron, respectively.

parameters employed in the present tight-binding calculations are the same as those reported in the band electronic structure studies of $K_{0.9}Mo_6O_{17}$[9] and $K_{0.3}MoO_3$.[7] In the following, we analyze how the crystal structure of $Li_{0.9}Mo_6O_{17}$ differs from that of $K_{0.9}$-Mo_6O_{17}, describe the band electronic structure of $Li_{0.9}Mo_6O_{17}$, and finally discuss some physical properties of $Li_{0.9}Mo_6O_{17}$.

Crystal Structure

As in the case of $K_{0.9}Mo_6O_{17}$,[9] it is convenient to describe the crystal structure of $Li_{0.9}Mo_6O_{17}$ in terms of the "building unit" Mo_4O_{21} (**1**), which is constructed from four MoO_6 octahedra by sharing the axial oxygen atoms. Shown in **2a** is a schematic representation of the Mo_4O_{15} layer, constructed from the Mo_4O_{21} chains, with the (11)(13)-condensation pattern: In a given pair of adjacent Mo_4O_{21} chains, the first MoO_6 octahedron of one chain is condensed with that of the other chain. For the next pair of adjacent Mo_4O_{21} chains, the first MoO_6 octahedron of one chain is condensed with the third MoO_6 octahedron of the other chain. The (11)(13)-Mo_4O_{15} layer **2a** may be represented by **2b** as well. Though not shown explicitly, every MoO_6 octahedron of **2** forms a zigzag Mo_2O_{10} chain **3** along the crystallographic *b*-axis. The Mo_4O_{15} layers found in $K_{0.9}Mo_6O_{17}$ have the (12)(12)-condensation pattern as depicted in **4**, where the first MoO_6 octahedron of one Mo_4O_{21} chain is condensed with the second MoO_6 octahedron of its adjacent Mo_4O_{21} chain.

When the outer MoO_6 octahedra of the (12)(12)-Mo_4O_{15} layer are condensed with MoO_4 tetrahedra, the Mo_6O_{17} layer found in $K_{0.9}Mo_6O_{17}$ results, where each MoO_4 tetrahedron belongs to only one $Mo_{14}O_{15}$ layer. In $Li_{0.9}Mo_6O_{17}$ as well, the outer MoO_6 octahedra of the (11)(13)-Mo_4O_{15} layer are condensed with MoO_4 tetrahedra. Unlike the case of $K_{0.9}Mo_6O_{17}$, however, there are two types of MoO_4 tetrahedra in $Li_{0.9}Mo_6O_{17}$. As schematically shown in Figure 1, one type of MoO_4 tetrahedra belongs to only one Mo_4O_{15} layer while the second type of MoO_4 tetrahedra joins two adjacent Mo_4O_{15} layers. Thus, unlike $K_{0.9}Mo_6O_{17}$, the $Li_{0.9}Mo_6O_{17}$ phase does not contain separated layers of composition Mo_6O_{17} but has a 3D crystal structure.

As indicated in **2a**, there are four different types of octahedral Mo atom sites in the (11)(13)-Mo_4O_{15} layer. How the d-electrons are distributed among the different Mo atoms of $Li_{0.9}Mo_6O_{17}$ is empirically estimated by performing a Zachariasen analysis[10] of the Mo–O bond lengths. This analysis reveals that the Mo atoms of the tetrahedral sites as well as the Mo^{III} and Mo^{IV} atoms of the octahedral sites have the oxidation state close to +6, but the Mo^{I} and Mo^{II} atoms of the octahedral sites have the oxidation state close to +5. Consequently, d-electrons, of $Li_{0.9}Mo_6O_{17}$ appear to be found only at the Mo^{I} and Mo^{II} sites, which form isolated double zigzag chains Mo_4O_{18} (**5a**) along the *b*-axis. A perspective view of **5a** along the *b*-axis can be depicted as in **5b**, and these Mo_4O_{18} chains are indicated by shading in **2a** and Figure 1. Therefore, $Li_{0.9}Mo_6O_{17}$ is 3D in crystal structure but is likely to be 1D in its electrical properties.[5a,e,f]

(8) Hoffmann, R. *J. Chem. Phys.* **1963**, *39*, 1397.
(9) Whangbo, M.-H.; Canadell, E.; Schlenker, C. *J. Am. Chem. Soc.* **1987**, *109*, 6308.
(10) Zachariasen, W. H. *J. Less-Common Metals* **1978**, *62*, 1.

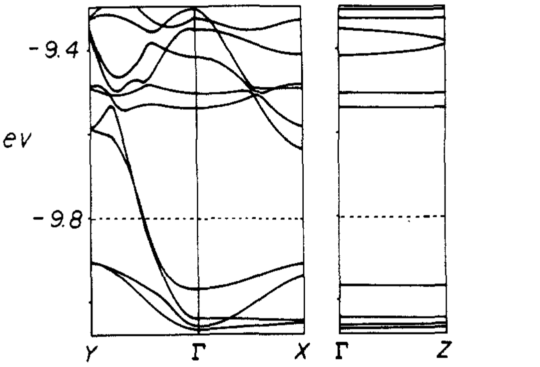

Figure 2. Dispersion relations of the d-block bands calculated for $Li_{0.9}Mo_6O_{17}$, where $\Gamma = (0,0,0)$, $X = (c^*/2,0,0)$, $Y = (0,b^*/2,0)$, and $Z = (0,0,a^*/2)$. The dashed line refers to the Fermi level.

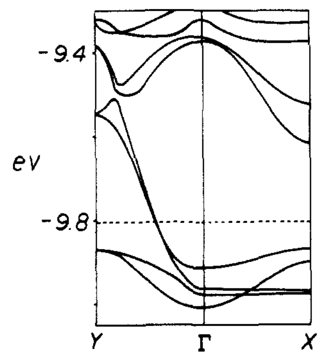

Figure 3. Dispersion relations of the d-block bands calculated for the Mo_6O_{24} layer, where the dashed line refers to the Fermi level.

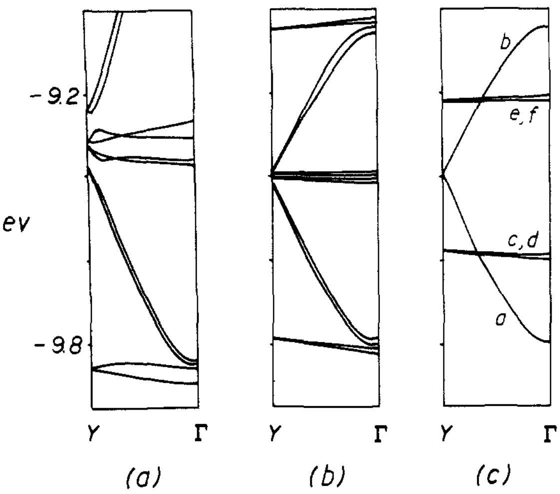

Figure 4. Dispersion relations of the d-block bands calculated for (a) the real Mo_4O_{18} chain, (b) the ideal Mo_4O_{18} chain, and (c) the ideal Mo_2O_{10} chain.

Band Electronic Structure

A. d-Block Bands. Shown in Figure 2 are the dispersion relations of the bottom d-block bands calculated for $Li_{0.9}Mo_6O_{17}$. With 5.8 electrons per unit cell $(Li_{0.9}Mo_6O_{17})_2$ to fill these d-block bands, two nearly degenerate 1D bands (dispersive primarily along the *b*-axis) become partially filled. In order to simplify our computational task we construct Mo_6O_{24} layers by removing from $Li_{0.9}Mo_6O_{17}$ all the MoO_4 tetrahedra and the MoO_6 octahedra containing Mo^{IV} atoms. Shown in Figure 3 are the bottom d-block bands calculated for one such Mo_6O_{24} layer. The bottom four d-block bands of Figure 3 are essentially identical with those of Figure 2. When the MoO_6 octahedra involving Mo^{III} atoms are removed from an Mo_6O_{24} layer, we obtain Mo_4O_{18} chains **5**. Figure 4a shows the bottom d-block bands of one Mo_4O_{18} chain **5**. It is quite clear from Figures 2, 3, and 4a that the bottom four

Chart I

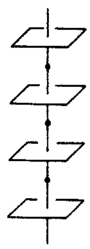

1

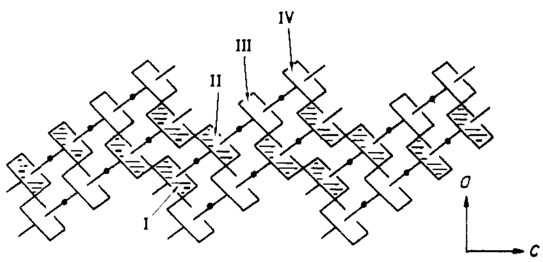

2a

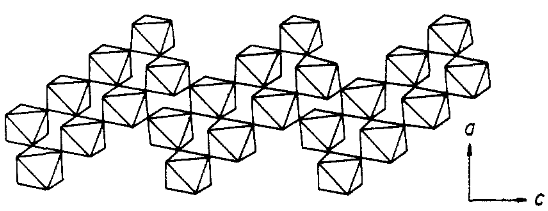

2b

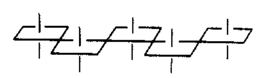

3

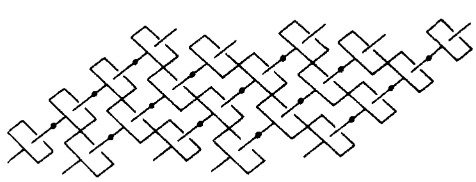

4a

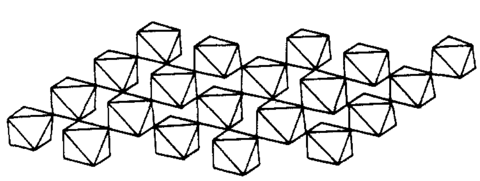

4b

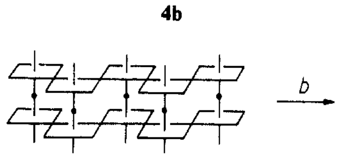

5a

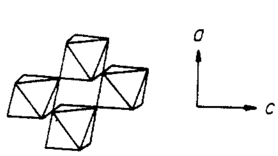

5b

d-block bands of $Li_{0.9}Mo_6O_{17}$ originate essentially from the Mo_4O_{18} chains.

Figure 5 shows the Fermi surfaces associated with the two partially filled d block bands of $Li_{0.9}Mo_6O_{17}$. The two Fermi surfaces are practically identical, and each one has a very good nesting vector $\mathbf{q} \simeq (0,0.45b^*,0)$.[11] As will be shown in the next section the two partially filled bands in the $\Gamma \rightarrow Y$ region of Figures 2 and 3 are related in orbital character to the two flat bands in the $\Gamma \rightarrow X$ region. The second and the fourth bands, from the bottom at Γ, avoid crossing each other on going from Γ to Y. The most striking feature of the band electronic structure of $Li_{0.9}Mo_6O_{17}$ is the 1D nature of its partially filled bands. Since this feature is so critical in interpeting various physical properties, let us first examine how the bottom d-block bands come about from the viewpoint of orbital interaction analysis.

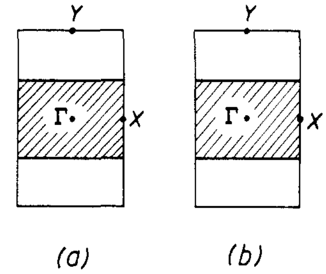

Figure 5. Fermi surfaces of the two partially filled d-block bands of $Li_{0.9}Mo_6O_{17}$. The wavevectors of the shaded and unshaded regions of the Brillouin zone give the occupied and unoccupied band levels. The Fermi surface is the boundary between the shaded and unshaded regions of wave vectors. Thus, each Fermi surface consists of two flat lines, and the upper piece is generated by translating the lower one with $\mathbf{q} \simeq (0,0.45b^*,0)$. Namely, the two pieces are nested by $\mathbf{q}$.

Chart II

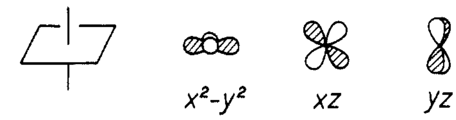

6

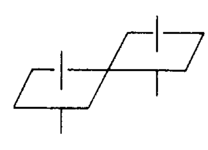

7a

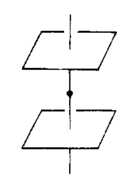

7b

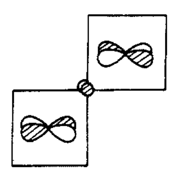

8a

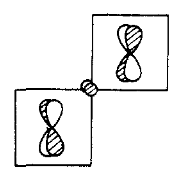

8b

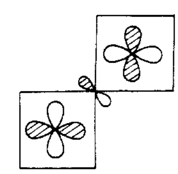

8c

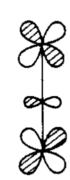

9a

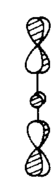

9b

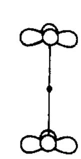

10

B. Band Formation. As described in the previous section, the bottom four d-block bands of $Li_{0.9}Mo_6O_{17}$ (two dispersive and two flat) originate largely from the Mo_4O_{18} chains **5**. In order to trace the origin of these bands, we perform tight-binding band calculations on the ideal Mo_4O_{18} double chain (i.e., the Mo_4O_{18} chain which is made up of regular MoO_6 octahedra). The t_{2g}-block

(11) With the formal oxidation $(Mo_6O_{17}^{0.9-})_2$ per unit cell, there are 5.8 electrons to fill the d-block bands. With four electrons in the two completely filled d-block bands, 1.8 electrons are left over to occupy the two partially filled d-block bands thereby leading to $\mathbf{q} \simeq (0, 0.45b^*, 0)$.

Table I. Antibonding Contributions of the Oxygen p-Orbitals of Mo–O–Mo Bridges in the t_{2g}-Block Band Orbitals of the Mo_2O_{10} Chain[a]

		bridging oxygen	
band orbital	wave vector	within a unit cell	between nearest-neighbor unit cells
11a	Γ	N	N
11b	Γ	Y	Y
12a	Y	N	Y
12b	Y	Y	N
13a	Γ	N	N
13b	Γ	N	N
14a	Y	N	N
14b	Y	N	N
15a	Γ	y	y
15b	Γ	y	y
16a	Y	y	y
16b	Y	y	y

[a] The presence of the antibonding contribution is indicated by the symbols Y or y, and the absence of it by the symbol N. The symbols Y and y refer to the stronger and the weaker antibonding contributions discussed in connection with **8** and **9**.

bands of this chain, shown in Figure 4b, are similar to those of the real Mo_4O_{18} chain (i.e., the Mo_4O_{18} chain found in $Li_{0.9}Mo_6O_{17}$) shown in Figure 4a. Note that the 12 t_{2g}-block bands of Figure 4b consist of three groups of flat bands and two groups of dispersive bands. Since the Mo_4O_{18} chain results from two Mo_2O_{10} chains **3** upon sharing their axial oxygen atoms, we calculated the t_{2g}-block bands of the ideal Mo_2O_{10} chain, which are shown in Figure 4c. It is clear from Figure 4 that the bottom two dispersive d-block bands of $Li_{0.9}Mo_6O_{17}$ originate from the dispersive band *a* of each Mo_2O_{10} chain, and the bottom two flat d-block bands of $Li_{0.9}Mo_6O_{17}$ originate from the flat bands *c* and *d* of each Mo_2O_{10} chain. Thus in the present section we will analyze the nature of the t_{2g}-block bands of the ideal Mo_2O_{10} and Mo_4O_{18} chains.

Interaction Patterns. For a given MoO_6 octahedron, its t_{2g}-block d orbitals may be shown as in **6**. It should be noticed that although not shown for simplicity, the orbitals of the surrounding oxygen atoms make antibonding contributions to the metal d orbitals. In constructing the Mo_2O_{10} and Mo_4O_{18} chains from MoO_6 octahedra, there occur two different kinds of oxygen atom bridging. As shown in **7a** and **7b**, two MoO_6 octahedra can be joined together by sharing either an "equatorial" or an "axial" oxygen atom. The Mo atoms of the Mo_2O_{10} and Mo_4O_{18} chains interact via the Mo–O–Mo bridges, so that the extent of dispersion of their d-block bands is governed by how strongly the p-orbitals of the bridging oxygen atoms interact with the Mo d-orbitals. In the bridging type of **7a**, the p-orbitals of the bridging oxygen atom combine out-of-phase with the two Mo atom d-orbitals when the latter two are in-phase as shown in **8**. The same interaction pattern occurs in the bridging type **7b** as well, as illustrated in **9a** and **9b** for the *xz* and *yz* orbitals, respectively. In the axial bridging **7b**, however, the Mo atom x^2-y^2 orbitals do not allow any participation of the bridging oxygen atom orbitals because they are δ-type orbitals with respect to the Mo–O–Mo axis (see **10**).

The molybdenum and oxygen orbitals are all in the same plane in **8c** and **9**, while this is not the case in **8a** and **8b**. Consequently, the extent of antibonding is greater in **8c** or **9** than in **8a** or **8b**. In the following, the presence of the strong metal–bridging ligand antibonding interaction as in **8c** or **9** will be denoted by the symbol Y, and that of weak metal–bridging ligand antibonding interaction as in **8a** or **8b** by the symbol y. In general, the sum of two weak metal–ligand antibonding interactions is equal in magnitude to one strong metal–ligand antibonding interaction (i.e., Y = 2y). When the metal d-orbitals combine out-of-phase in **8** and **9**, no orbitals of the bridging oxygen atom can mix with the d-orbitals. In such a case, there is no metal–bridging ligand antibonding interaction, which can be denoted by the symbol N.

Ideal Mo_2O_{10} Chain. The t_{2g}-block d-bands of the ideal Mo_2O_{10} chain are shown in Figure 4c. The orbitals of the dispersive bands *a* and *b* at Γ are given by **11a** and **11b**, respectively, and those

Chart III

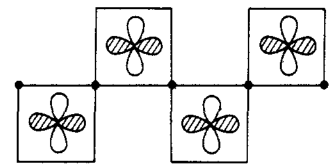

11a

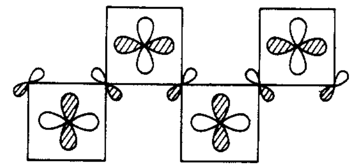

11b

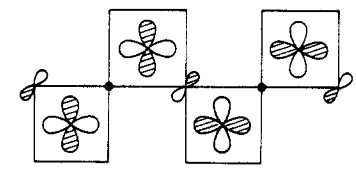

12a

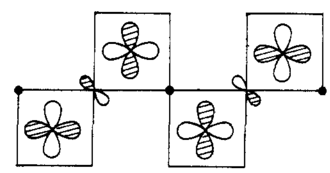

12b

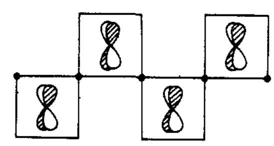

13a

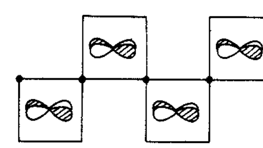

13b

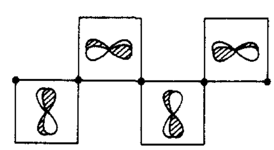

14a

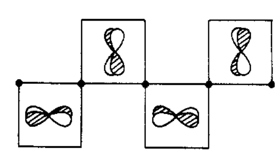

14b

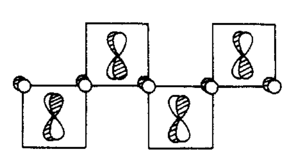

15a

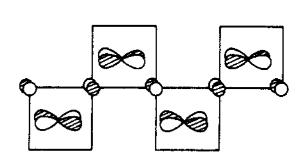

15b

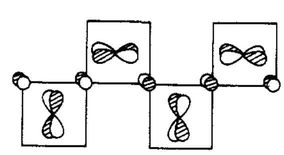

16a

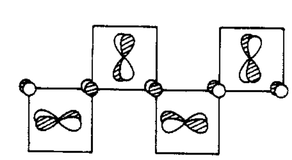

16b

at Y by **12a** and **12b**, respectively. The metal–bridging ligand antibonding interactions present in **11** and **12** are summarized in Table I. Note that the dispersion of the band *a* covers the energy change from **11a** to **12a**, and that of the band *b* covers the energy change from **11b** to **12b**. Since **12a** and **12b** are degenerate, the two bands *a* and *b* merge at Y.

The orbitals of the two lower flat bands *c* and *d* of Figure 4c are given by **13** at Γ and by **14** at Y. Similarly, the orbitals of the two upper flat bands *e* and *f* are given by **15** at Γ and by **16** at Y. The metal–bridging ligand antibonding interactions present in **13–16** are listed in Table I. The bands *c* and *d* are flat since the orbitals of the bridging oxygen atoms do not mix into the d orbitals both at Γ and at Y, while the bands *e* and *f* are flat because the orbitals of the bridging oxygen atoms mix with the d orbitals both at Γ and at Y.

According to Table I alone in which one considers only the metal–bridging ligand antibonding interactions, the energy level of **11a** would be similar to that of either **13a** or **13b**. That **11a** is lower in energy than either **13a** or **13b** arises from the difference in the extent of the molybdenum–nonbridging oxygen atom antibonding interactions. Each Mo atom of the Mo_2O_{10} chain has four (two axial and two equatorial) unshared oxygen atoms. As depicted in **17**, the two equatorial oxygen atoms provide two strong Mo–O antibonding interactions to the x^2-y^2 orbital but two weak Mo–O antibonding interactions to the xz and yz orbitals. As shown in **18**, however, the two axial oxygen atoms do not contribute to the x^2-y^2 orbital but contribute two strong Mo–O antibonding interactions to the xz and yz orbitals. Since the sum of the two weak Mo–O antibonding corresponds to one strong Mo–O antibonding, the overall antibonding contribution of the four unshared oxygen atoms is stronger in **13a** or **13b** than in **11a**. In a similar manner, it can be easily shown that the flat bands *c* and *d* lie in the middle of the band *a*, and the flat bands *e* and *f* lie in the middle of the band *b*.

Ideal Mo_4O_{18} Chain. The t_{2g}-block bands of the ideal Mo_4O_{18} chain are shown in Figure 4b. The Mo_4O_{18} chains are obtained from two Mo_2O_{10} chains by sharing the axial oxygen atoms. As discussed in the previous section, the x^2-y^2 orbital of each MoO_6 octahedron (i.e., **18a**) gives rise to the dispersive bands *a* and *b* of the Mo_2O_{10} chain. The x^2-y^2 orbital of an MoO_6 octahedron has no orbital contribution from the axial oxygen atoms. Thus, if two MoO_6 octahedra are joined together to make an Mo_2O_{11} unit by sharing an axial oxygen atom, the in-phase and out-of-phase combinations (**19a** and **19b**, respectively) of the two x^2-y^2 orbitals are practically degenerate. Therefore, the dispersive bands *a* and *b* of the Mo_2O_{10} chain would remain the same in the Mo_4O_{18} chain. This explains the existence of the nearly degenerate, dispersive bands in Figure 4b.

The xz and yz orbitals (i.e., **18b** and **18c**, respectively) of each MoO_6 octahedron, which lead to the flat bands *c*–*f* of the ideal Mo_2O_{10}, have p-orbital participation from the axial oxygen atoms. How the energy level of **18b** (or **18c**) of an MoO_6 octahedron is affected upon making an Mo_2O_{11} unit by sharing an axial oxygen atom is depicted in **20** with the xz orbital as an example. The $(xz)_-$ orbital **21a** is lower in energy than the xz level, since the orbital of the bridging oxygen atom does not mix into the $(xz)_-$. The $(xz)_+$ orbital **21b** is higher in energy than the xz level, since the p-orbital of the bridging oxygen atom mixes in with a greater coefficient than in the case of an MoO_6 octahedron **18b** (this makes the $(xz)_+$ orbital normalized to unity). The set of the bands *c* and *d* and that of the bands *e* and *f* each undergo the kind of level splitting depicted in **22**, when two Mo_2O_{10} chains are condensed into one Mo_4O_{18} chain. Consequently, the two groups of nearly degenerate bands in each Mo_2O_{10} chain give rise to the four groups of nearly degenerate bands, as depicted in **22**. As a result, we obtain the 12 t_{2g}-block d-bands of the ideal Mo_4O_{18} chain shown in Figure 4b. As can be seen from Figure 4, parts a and b, the d-block bands of the real Mo_4O_{18} chain are only slightly different from those of the ideal Mo_4O_{18} chain, which reflects the fact that in the real Mo_4O_{18} chain, each MoO_6 octahedron deviates somewhat from a regular octahedral structure.

Interchain Interactions. It is clear from the above that the four filled d-block bands of $Li_{0.9}Mo_6O_{17}$ (Figures 2–4) arise primarily from the Mo_4O_{18} chains (**5**) parallel to the *b*-axis. As can be seen from **2a**, the Mo_4O_{18} chains are linked to one another via the MoO_6 octahedra involving the Mo^{III} atoms. Note that each $Mo^{III}O_6$ octahedron is linked to two Mo_4O_{18} chains, one with sharing its axial oxygen atom and the other with sharing its equatorial oxygen atom. The x^2-y^2 orbital of each Mo^{II} atom makes a δ-type overlap interaction (see **10**), and hence practically no overlap interaction, with the $Mo^{III}O_6$ octahedron through the shared axial oxygen atom. As far as the x^2-y^2 orbitals of the Mo^{II} atoms are concerned, therefore, the Mo_4O_{18} chains of $Li_{0.9}Mo_6O_{17}$ do not interact with

Chart IV

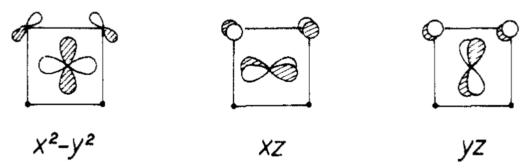

17a **17b** **17c**

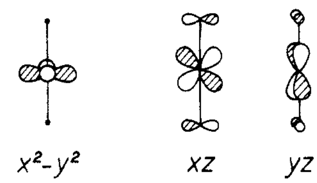

18a **18b** **18c**

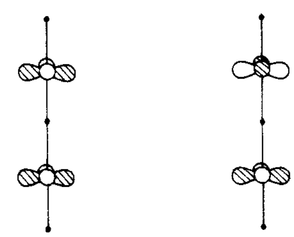

19a **19b**

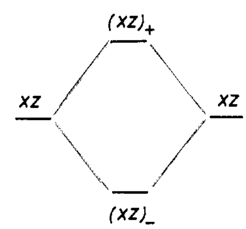

20

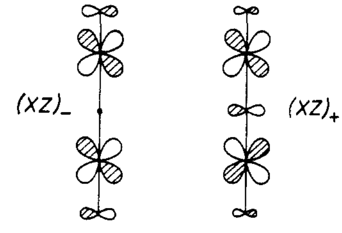

21a **21b**

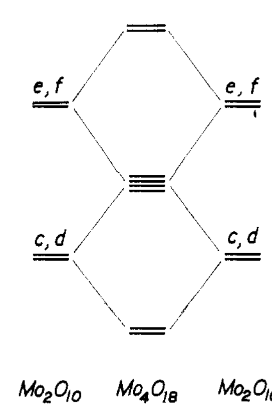

22

one another. Consequently, the lower two dispersive bands of a single Mo_4O_{18} chain retain their 1D character in 3D $Li_{0.9}Mo_6O_{17}$.

Each $Mo^{III}O_6$ octahedron provides a π-type overlap interaction not only with the Mo^{II} atom xz/yz orbitals through the shared equatorial oxygen atom (e.g., **8a**–**8c**) but also with those through the shared axial oxygen atom (e.g., **9a** and **9b**). That is, as far as the xz/yz orbitals of the Mo^{II} atoms are concerned, the Mo_4O_{18} chains of $Li_{0.9}Mo_6O_{17}$ do interact to one another. This explains why two of the bottom four bands in $Li_{0.9}Mo_6O_{17}$ are almost equally dispersive, though not strongly, along the $\Gamma \rightarrow X$ and $\Gamma \rightarrow Y$ directions.

Fermi Surfaces and Physical Properties

It was shown in the previous section that $Li_{0.9}Mo_6O_{17}$ has two completely filled and two partially filled d-block bands, which are all derived from the t_{2g}-orbitals of the MoO_6 octahedra belonging to the Mo_4O_{18} chains. The two partially filled d-block bands are dispersive only along the Mo_4O_{18} chain direction, and their dispersion curves along that direction are essentially degenerate in the region of the Fermi level. Hence the result is two almost identical Fermi surfaces shown in Figure 5, where each Fermi surface is open so that $Li_{0.9}Mo_6O_{17}$ is expected to be a 1D metal in agreement with the prediction based upon the Zachariasen analysis.[10] The two pieces of each Fermi surface in Figure 5 are flat and thus are perfectly nested by the wave vector $\mathbf{q} \cong (0,0.45b^*,0)$. Consequently, $Li_{0.9}Mo_6O_{17}$ is expected to be susceptible to a 1D instability such as charge density wave (CDW) or spin density wave (SDW) formation associated with $\mathbf{q}$.[12]

The electrical resistivity of $Li_{0.9}Mo_6O_{17}$ decreases slowly as temperature is lowered down to 25 K, below which the resistivity gradually increases until it drops abruptly to zero around 1.9 K.[5] The resistivity upturn at 25 K may be due to a CDW formation, as suggested by Greenblatt et al.[5c] According to Fröhlich, sliding CDWs can lead to superconductivity.[13] In general, the Fröhlich superconductivity is not observed because of CDW pinning[14] that gives rise to nonlinear electrical conductivity.[13c,15] If a CDW is responsible for the resistivity upturn at 25 K, therefore, the absence of nonlinear conductivity in $Li_{0.9}Mo_6O_{17}$[16] implies that CDW pinning does not occur in this compound. Then, one may speculate that the superconductivity at 1.9 K might be a consequence of the Fröhlich mechanism instead of the regular (i.e., non-Fröhlich) mechanism.[17] However, we note that $(Li_{1-x}Na_x)_{0.9}Mo_6O_{17}$ ($x \leq 0.48$) and $(Li_{1-x}K_x)_{0.9}Mo_6O_{17}$ ($x \leq 0.40$) exhibit both the resistivity upturn around 25 K and the superconductivity below 2 K[5d,e] despite random potentials expected from the presence of mixed alkali cations. Alternatively, therefore, it may be suggested that the resistivity upturn of $Li_{0.9}Mo_6O_{17}$ at 25 K is caused by a SDW formation in the Mo_4O_{18} chains by analogy with the SDW $\rightarrow$ superconductor transition in the 1D organic metal $(TMTSF)_2PF_6$, although the latter occurs only under pressure.[18] The magnetic susceptibility of $Li_{0.9}Mo_6O_{17}$ is observed to remain nearly constant upon lowering temperature below 25 K.[5c] This observation is consistent with the possibility of a SDW instability rather than with that of a CDW instability as a cause for the resistivity upturn at 25 K.

Concluding Remarks

Both $K_{0.9}Mo_6O_{17}$ and $Li_{0.9}Mo_6O_{17}$ are constructed from MoO_6 octahedra and MoO_4 tetrahedra by sharing their oxygen corners. The Mo_4O_{15} layers of MoO_6 octahedra in both compounds can be considered as a condensation product of the Mo_4O_{21} chains. These octahedral Mo_4O_{15} layers have the (12)(12)- and (11)-(13)-condensation patterns in $K_{0.9}Mo_6O_{17}$ and $Li_{0.9}Mo_6O_{17}$, respectively. The outer MoO_6 octahedra of the octahedral Mo_4O_{15} layers are capped by MoO_4 tetrahedra in $K_{0.9}Mo_6O_{17}$ and $Li_{0.9}Mo_6O_{17}$. In $K_{0.9}Mo_6O_{17}$ the MoO_4 tetrahedra are not shared by adjacent octahedral Mo_4O_{15} while in $Li_{0.9}Mo_6O_{17}$ one-half of the MoO_4 tetrahedra are shared by two adjacent octahedral Mo_4O_{15} layers. Therefore, the crystal structures of $K_{0.9}Mo_6O_{17}$ and $Li_{0.9}Mo_6O_{17}$ are 2D and 3D, respectively. Nevertheless, the electrical properties of $Li_{0.9}Mo_6O_{17}$ are more anisotropic than those of $K_{0.9}Mo_6O_{17}$, which is 2D. This arises from the fact that the partially filled d-block bands of $Li_{0.9}Mo_6O_{17}$ are primarily represented by the Mo_4O_{18} chains embedded in each octahedral Mo_4O_{15} layer. The obvious reason for this observation is that the MoO_6 octahedra of the Mo_4O_{18} chains have longer Mo–O bonds than do other MoO_6 octahedra and MoO_4 tetrahedra, and hence have lower lying d-block bands.[9]

Our band orbital analysis shows that the bottom d-block bands of $Li_{0.9}Mo_6O_{17}$ are primarily derived from the t_{2g}-block bands of the Mo_4O_{18} chains. Of the four filled d-block bands of $Li_{0.9}Mo_6O_{17}$, two are dispersive along the chain direction and partially filled. Each of these two gives rise to a 1D Fermi surface nested by the vector $\mathbf{q} \cong (0,0.45b^*,0)$, so that $Li_{0.9}Mo_6O_{17}$ is expected to be susceptible to either CDW or SDW formation. The present study raises a couple of interesting questions concerning $Li_{0.9}Mo_6O_{17}$: (a) whether the resistivity upturn at 25 K is caused by a CDW or an SDW, and (b) whether the superconductivity at 1.9 K is due to the Fröhlich mechanism or not. To resolve these questions, it is necessary to carry out further experimental studies on $Li_{0.9}Mo_6O_{17}$ (e.g., measurements of diffuse X-ray scattering and specific heat capacity).

Acknowledgment. This work was supported by NATO, Scientific Affairs Division, and also by DOE, Office of Basic Sciences, Division of Materials Sciences, under Grant DE-FG05-86-ER45259. The authors express their appreciation for computing time on the ER-Cray X-MP computer, made available by the DOE. M.-H.W. would like to thank Prof. M. Greenblatt, Prof. M. Sato, and Prof. C. Schlenker for their reprints and preprints. M.-H.W. is also grateful to Prof. M. Greenblatt and Dr. R. M. Fleming for invaluable discussions.

Registry No. $Li_{0.9}Mo_6O_{17}$, 106770-42-7.

(12) Horovitz, B.; Gutfreund, H.; Weger, M. *Phys. Rev. B* **1975**, *8*, 3174.

(13) (a) Fröhlich, H. *Proc. R. Soc. London, Ser. A* **1954**, *223*, 296. (b) Allender, D.; Bray, J. W.; Bardeen, J. *Phys. Rev. B* **1974**, *9*, 119. (c) Monceau, P. In *Electronic Properties of Inorganic Quasi-One-Dimensional Compounds*, Part II; Monceau, P., Ed.; Reidel: Dordrecht, The Nertherlands, 1985; p 139.

(14) Lee, P.; Rice, T. M.; Anderson, P. W. *Solid State Commun.* **1974**, *14*, 703.

(15) (a) Rouxel, J. In *Crystal Structures and Properties of Materials with Quasi-One-Dimensional Structures*; Rouxel, J., Ed.; Reidel: Dordrecht, The Netherlands, 1986; p 1. (b) Moret, R.; Pouget, J. P. *Ibid.* p 87. (c) Schlenker, C.; Dumas, J. *Ibid.* p 135. (d) Meerschaut, A.; Rouxel, J. *Ibid.* p 222. (e) Monceau, P. *Physica* **1982**, *109, 110B*, 1890. (f) Fleming, R. M. *Physics in One Dimension, Solid State Sciences*; Bernasconi, J., Schnieder, T., Eds.; Springer-Verlag: Berlin, 1981; Vol. 23, p 253. (g) Grüner, G. *Physica* **1983**, *8D*, 1.

(16) Greenblatt, M., private communication.

(17) (a) Bardeen, J.; Cooper, L. N.; Schriefer, J. R. *Phys. Rev.* **1957**, *106*, 162; **1957**, *108*, 1175. (b) McMillan, W. L. *Phys. Rev.* **1968**, *167*, 331. (c) Mathias, B. T. In *Superconductivity*; Wallace, P. R., Ed.; Gordon and Breach, Science Publishers: New York, 1969; Vol. 1, p 227.

(18) (a) Jérome, D.; Mazaud, A.; Ribault, M.; Bechgaard, K. *J. Phys. Lett. (Les Ulis, Fr.)* **1980**, *41*, L195. (b) Torrance, J. B.; Pedersen, H. J.; Bechgaard, K. *Phys. Rev. Lett.* **1982**, *49*, 881. (c) Walsh, W. M., Jr.; Wudl, F.; Thomas, G. A.; Nalewajek, D.; Hauser, J. J.; Lee, P.; Poehler, T. O. *Phys. Rev. Lett.* **1980**, *45*, 829. (d) Pouget, J. P.; Moret, R.; Comes, R.; Shirane, G.; Bechgaard, K.; Fabre, J. M. *J. Phys. (Les Ulis, Fr.)* **1983**, *43*, C3-969. (e) Scott, J. C.; Pederson, H. J.; Bechgaard, K. *Phys. Rev. Lett.* **1980**, *45*, 2125.